Scripta Materialia 154 (2018) 192–196

Contents lists available at ScienceDirect

Scripta Materialia

journal homepage: www.elsevier.com/locate/scriptamat

Regular article

Interphase boundary segregation of silver and enhanced precipitation of $Mg_{17}Al_{12}$ Phase in a Mg-Al-Sn-Ag alloy

Jiashi Miao [a], Weihua Sun [a], Andrew D. Klarner [a], Alan A. Luo [a,b,*]

[a] Department of Materials Science and Engineering, The Ohio State University, Columbus, OH 43210, USA
[b] Department of Integrated Systems Engineering, The Ohio State University, Columbus, OH 43210, USA

ARTICLE INFO

Article history:
Received 7 April 2018
Received in revised form 23 May 2018
Accepted 29 May 2018
Available online xxxx

Keywords:
Magnesium alloys
$Mg_{17}Al_{12}$ precipitate
Enhanced aging hardening response
Segregation
Ag addition

ABSTRACT

Aging-hardening response of Mg-7Al-2Sn (wt%) alloy can be remarkably accelerated by a small addition of silver (Ag). Using high-angle annular dark-field scanning transmission electron microscopy (HAADF-STEM) coupled with high resolution energy dispersive X-ray spectroscopy (EDS) mapping, for the first time, segregation of solute atoms (Ag in this case) was observed at the interphase boundary between continuous $Mg_{17}Al_{12}$ precipitate and magnesium matrix in Mg-7Al-2Sn alloy with 0.7 wt% Ag addition. Substantial size refinement and increased number density of $Mg_{17}Al_{12}$ precipitates may be responsible for the enhanced aging-hardening response in Mg-7Al-2Sn alloy with Ag addition.

Magnesium alloys have attracted great interests due to the increasing demands for weight reduction and fuel efficiency in the automotive and aerospace industries [1,2]. One major limitation of commercial magnesium alloys is their low strength. Precipitation hardening is one of the most efficient ways to improve the strength of magnesium alloys, especially those targeted for casting applications [3]. Aluminum, with a large solubility up to 12 wt% in magnesium at around 437 °C, has been frequently added to commercial AZ (Mg-Al-Zn) and AM (Mg-Al-Mn) serial magnesium alloys as one principal alloying element. Upon cooling from high temperatures and aging at low temperatures, $Mg_{17}Al_{12}$ phase with a complex body centered cubic structure can form in Mg—Al based alloys through two competitive and simultaneous reactions: continuous precipitation and discontinuous precipitation [4,5]. Continuous precipitation nucleates and grows within grain interior, leading to a continuous change in the composition in magnesium matrix, while discontinuous precipitation forms through cellular growth at grain boundaries. $Mg_{17}Al_{12}$ phase has an Burgers orientation relationship ($(0001)_{Mg}//(011)_{Mg17Al12}$, $[2\bar{1}\,\bar{1}0]_{Mg}//[1\bar{1}1]_{Mg17Al12}$) with respect to magnesium matrix [6,7]. Mg—Al based alloys have poor mechanical properties especially at elevated temperatures, mainly due to softening of discontinuous $Mg_{17}Al_{12}$ at grain boundaries. The addition of Sn to magnesium leads to the formation of Mg_2Sn precipitate with a face centered cubic crystal structure [8]. As compared with $Mg_{17}Al_{12}$ phase, Mg_2Sn has a higher melting point of 770 °C, thus having a better thermal stability. Sn addition also can effectively reduce the formation discontinuous precipitates $Mg_{17}Al_{12}$ at grain boundaries, further improving alloy stability at elevated temperatures. Previous study of different Mg-Al-Sn system shows that Mg-7Al-2Sn, designated AT72, has an excellent combination of strength, ductility and corrosion resistance among different Mg-Al-Sn alloys [9].

However, one main drawback of using Mg_2Sn phase for the purpose of precipitation hardening is that its precipitation kinetics is very sluggish and thus aging hardening response is poor. Addition of Zn can substantially increase aging hardening of Mg—Sn alloys through refining Mg_2Sn precipitates and increasing its number density [10,11]. A recent study using advanced scanning transmission electron microscopy (STEM) coupled with energy-dispersive X-ray spectroscopy (EDXS) reveals that Zn can segregate at the interface boundary between Mg_2Sn precipitates and Mg matrix in Mg—Zn alloys [12]. Such segregation may play an important role in enhancing aging hardening response in Mg—Sn systems. Mechanical properties of magnesium alloys can be greatly influenced by the segregation of alloying elements. For example, in Mg—Gd, Mg—Zn and Mg-Gd-Zn alloys, periodic equilibrium segregation of solutes are observed at fully coherent twin boundaries, leading to unusual annealing strength through the pinning effects of solutes at twin boundaries [13].

Silver is an effective alloying element for improving the strength of Mg alloys, and it can substantially enhance aging hardening response in Mg-Y-Zn alloys, through promoting the formation of the densely distributed basal precipitates [14]. Enhanced aging hardening response and significant refinement of precipitation microstructure was observed

* Corresponding author.
E-mail address: luo.445@osu.edu (A.A. Luo).

https://doi.org/10.1016/j.scriptamat.2018.05.047
1359-6462/

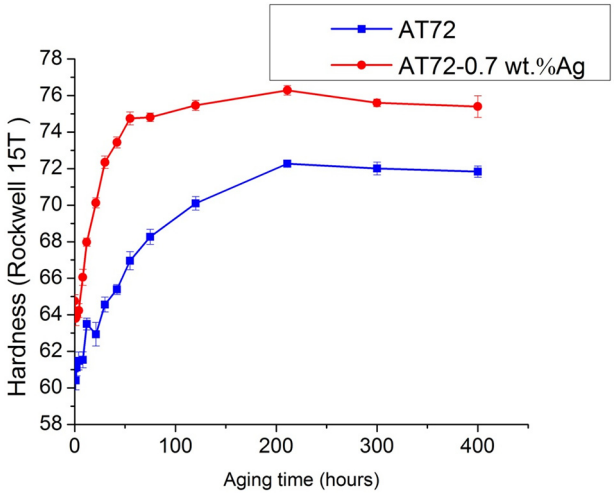

Fig. 1. Aging hardening response of AT72 alloys with and without Ag addition during isothermal aging at 200 °C.

in Mg-2.4 at.% Zn alloy with the addition of trace amount of Ag and Ca [15]. The addition of Ag and Zn in Mg—Gd alloys results in the formation of nano-scale precipitates and thus significantly improve aging hardening response [16]. Similar enhanced aging hardening response due to Ag addition was also observed in other Mg alloys systems including Mg—Gd alloys [17] and Mg—5Sn alloy [18].

In this work, the effect of Ag addition on aging hardening response of AT72 alloy was investigated. Advanced transmission electron microscopy including atomic resolution high-angle annular dark-field (HAADF) scanning transmission electron microscopy coupled with high resolution EDS mapping were used to reveal detailed precipitation microstructure, especially the chemistry of the interphase boundaries. Such detailed microstructure characterization provides valuable insights to the understanding of the effect of addition of micro-alloying elements on precipitation kinetics and mechanical properties of Mg alloys.

Test alloy ingots (25 mm in diameter) with nominal compositions of Mg–7Al–2Sn and Mg-7Al-2Sn-0.7 wt% Ag were prepared through induction melting in a mild steel crucible under a protection atmosphere of 0.5%SF_6/CO_2, and casting into a steel cylinder mold. Samples cut from ingots were solution treated at 420 °C for 24 h, and then water quenched. Aging treatment was carried out in a silicone oil bath at 200 °C. Hardness tests were conducted on a Buehler Rockwell hardness tester using Rockwell superficial 15T scale. For each aging condition, a total of 10 measurements were recorded. Thin slices with a thickness around 800 μm were cut from aging specimens using a low speed diamond saw. Those specimens were mechanically ground to about 90 μm. Further mechanical polishing down to about 30 μm was conducted in a Finisone 100 dimpler. Final perforation of thin TEM foils were completed using a Finione model 1010 ion mill. Quantitative precipitation characterization was conducted using a FEI Tecnai TF20 microscope operating at an accelerating voltage of 200 keV. For each dimension of $Mg_{17}Al_{12}$ precipitates, about 250 precipitates were measured. The

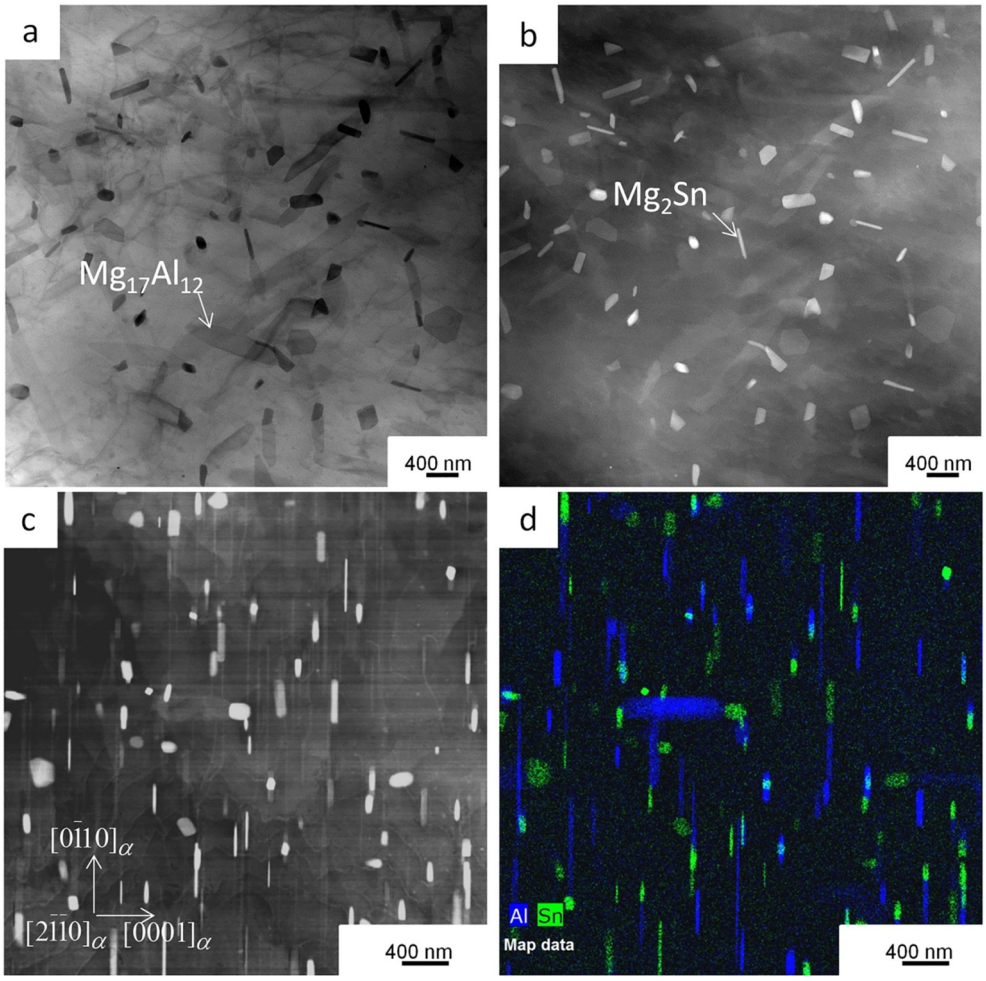

Fig. 2. STEM characterization of precipitation microstructure in AT72 alloy after isothermal aging at 200 °C for 55 h: a) BF-STEM image (beam close to [0001] zone axis); b) corresponding HAADF-STEM image; c) HAADF-STEM image showing the region for EDS mapping (α represents Mg matrix); and d) Al EDS map overlapped with Sn map.

length and width of $Mg_{17}Al_{12}$ were measured on BF-STEM images along basal orientation, while the thickness of $Mg_{17}Al_{12}$ was measured on BF-STEM images along $[2\bar{1}\ \bar{1}0]$ zone axis. The thickness of TEM foils for the calculation of number density was determined using electron energy loss spectroscopy (EELS). Due to the wedge shape of TEM foils prepared by ion milling method and large size of $Mg_{17}Al_{12}$ precipitates, large uncertainty may be associated with precipitate number density measurement. To further verify the number density measurement, two lift-out TEM specimens for AT72 alloy and AT72–0.7 wt% Ag alloy after aging at 200 °C for 55 h were prepared using FEI Helios focused ion beam system. The normal of TEM foils was within 2 degrees away from basal orientation. The wedge shape effect associated with ion milled TEM specimens can be greatly reduced in FIB TEM specimens, and the thickness of FIB foils can be directly measured using SEM imaging or ion beam imaging. Atomic resolution HAADF-STEM imaging was carried out on a FEI G2 80–300 TEM/STEM equipped with a Cs probe corrector. EDS mapping was conducted in a FEI G2 60–300 TEM/STEM microscope equipped with a Super-X EDS system with four windowless silicon-drift detectors.

Fig. 1 shows the aging hardening response of AT72 alloy with and without Ag addition at 200 °C. The hardness value of as-quenched AT72 alloy with Ag addition is about 64 HR 15 T, which is higher than that of the base alloy without Ag addition. As shown in Fig. 1, the aging hardening response of AT72 alloy is sluggish, with slow increase of hardness with aging time. On the contrary, the hardness of AT72 alloy with Ag addition increases very rapidly, indicating remarkably accelerated age hardening response. Furthermore, AT72 alloy with 0.7 wt % Ag addition shows a peak hardness of about 76 HR 15T, which is also higher that of AT72 base alloy.

To reveal the mechanisms associated with the observed enhanced aging hardening response, detailed TEM characterization was conducted on AT72 alloy with and without Ag addition after aging at 200 °C for 55 h. This aging condition corresponds to an under-aged condition, but very close to peak aging condition of AT72 alloy with 0.7 wt% Ag addition.

Figs. 2 a) and b) are low-magnification bright-field STEM (BF-STEM) and corresponding HAADF-STEM images of AT72 alloy after aging for 55 h. There are two groups of precipitates in AT72 alloy: $Mg_{17}Al_{12}$ and Mg_2Sn. Most of $Mg_{17}Al_{12}$ precipitates have a lozenge shape as shown in Fig. 2 a), while the rest has a lath shape. Most $Mg_{17}Al_{12}$ precipitates have a Burgers orientation relationship with respect to magnesium matrix. The morphology of Mg_2Sn precipitates are shown in Fig. 2 b). It is well known that HAADF-STEM image contrast is proportional to the square of atomic number [19]. Therefore, Mg_2Sn precipitates have higher image contrast as compared with either Mg matrix or $Mg_{17}Al_{12}$ precipitates in HAADF-STEM images. Both groups of precipitates can be easily identified by combining BF/HAADF image pair as shown in Fig. 2a) and b). Some Mg_2Sn precipitates are of lath shape, while others have irregular morphology. Fig. 2c) is a HAADF-STEM image showing the region for EDS mapping. Fig. 2d) is Al element map overlapped with Sn map. It can be seen that the sizes of $Mg_{17}Al_{12}$ precipitates are considerably larger than those of Mg_2Sn precipitates.

Fig. 3 is a low magnification BF-STEM image along $[2\bar{1}\ \bar{1}0]$ zone axis of magnesium matrix showing the precipitation microstructure in AT72 with 0.7 wt% Ag addition, after aging at 200 °C for 55 h. Most $Mg_{17}Al_{12}$ precipitates in AT72 alloy with 0.7 wt% Ag addition still maintain Burgers orientation relationship with matrix, indicating that the small addition of Ag does not change the orientation relationship between $Mg_{17}Al_{12}$ precipitates and magnesium matrix. An HAADF-STEM image and corresponding EDS maps are given in Fig. 3 b) and c), respectively. The EDS map shows a much higher density of $Mg_{17}Al_{12}$ precipitates in the Ag-containing alloy. The HAADF-STEM image in Fig. 3 d) shows

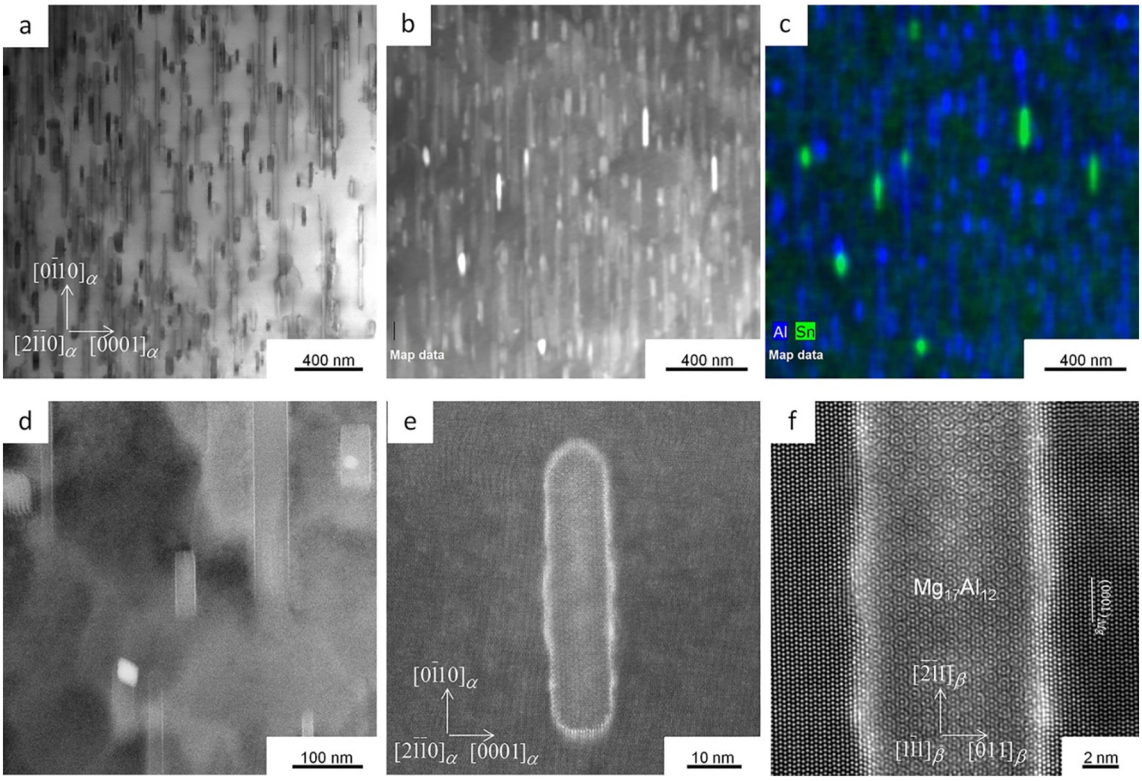

Fig. 3. STEM characterization of precipitation microstructure in AT72 alloy with 0.7 wt% Ag addition: a) BF-STEM image along the $[2\bar{1}\ \bar{1}0]$ zone axis of magnesium; b) HAADF-STEM image showing the region for EDS map; c) Al EDS map overlapped with Sn map; d) HAADF-STEM image showing high contrast at regions close to interphase boundaries of $Mg_{17}Al_{12}$ precipitates; e) HAADF-STEM image of a single $Mg_{17}Al_{12}$ precipitates; and f) atomic resolution HAADF-STEM image of the interface boundary between $Mg_{17}Al_{12}$ and magnesium matrix (β represents $Mg_{17}Al_{12}$ precipitate).

that the region close to the interface between $Mg_{17}Al_{12}$ precipitate and magnesium matrix has higher contrast as compared with magnesium matrix. This phenomenon appears more apparent in Fig. 3 e), which just shows a single $Mg_{17}Al_{12}$ precipitate. Results in Fig. 3 d) and e) indicate potential segregation of heavy elements at regions close to interface boundaries. Fig. 3 f) shows an atomic resolution HAADF-STEM image along the $[2\bar{1}\,\bar{1}0]$ zone axis of magnesium. It can be seen that solute segregate not only at both the broad interfaces parallel to the $(0001)_{Mg}$ habit plane but also along the side interfaces and the tips of precipitates. The regions with high image contrast extend to several atomic planes away from the interphase boundaries rather than just localize at interfaces. There is no trend of site specific segregation or ordering observed at interface.

High resolution STEM EDS mapping was used to identify the type of solutes segregating at interface regions. Fig. 4 a) is a HAADF-STEM image showing the region where EDS mapping was collected. Similar to results presented in Fig. 3 d)-f), in the HAADF-STEM image, the regions close to interface has much higher contrast. Fig. 4 b)-c) are EDS maps of Al and Ag respectively. It can be seen from Fig. 4 c), Ag segregates at the interface boundary. Fig. 4 d) show integrated EDS composition profiles across the precipitates and interphase boundaries as illustrated in Fig. 4 c). It clearly shows that Ag segregate at interface, while there is no large difference of Sn content at region close to interface and region far away from interface. Therefore, high image contrast at interphase boundary regions in HAADF-STEM images originates from Ag segregation. The Ag content in $Mg_{17}Al_{12}$ is also higher than magnesium matrix, indicating some solubility of Ag in $Mg_{17}Al_{12}$ precipitates. On the contrary, Sn content in $Mg_{17}Al_{12}$ is fairly low, indicating low solubility of Sn in $Mg_{17}Al_{12}$ precipitates. Similar interphase boundary segregation of Ag was also observed at both broad interfaces and side interfaces between $Mg_{17}Al_{12}$ precipitate and magnesium matrix after longer aging time (205 h) in AT72–0.7.wt% Ag alloy. Further HAADF-STEM imaging of AT72-0.7 wt% Ag sample after short time (1 h and 2 h) did not reveal the formation of Ag mono-layer or multi-layer in magnesium matrix.

Three dimensional sizes and number density of continuous $Mg_{17}Al_{12}$ precipitates are quantitatively measured for both AT72 and AT72-0.7 wt % Ag alloys after isothermal aging at 200 °C for 55 h. The main results are summarized in Table 1. All three dimensional sizes of $Mg_{17}Al_{12}$ precipitates in AT72 alloy with Ag addition are substantially smaller than those in the base alloy. Especially, the width and length of precipitates in AT72 alloy with Ag addition are just one third of those in the base alloy, indicating that Ag addition can remarkably refine continuous $Mg_{17}Al_{12}$ precipitates. The number density of $Mg_{17}Al_{12}$ in Ag addition alloy measured from both ion milling TEM foils and FIB lift-out TEM foils is also about one order of magnitude higher than that of AT72 base alloy. The number density of Mg_2Sn in both alloys are close and around $6/\mu m^3$. Therefore, $Mg_{17}Al_{12}$ is the main strengthening precipitate phase in AT72 alloys with Ag addition. The enhanced aging response in Ag addition alloy may be due to the refined and higher number density of $Mg_{17}Al_{12}$ precipitates.

It has been reported that Ag addition can effectively improve the strength of aging-hardenable light alloys such as magnesium [20,21] and aluminum [22–24] alloys. Enhanced aging hardening response

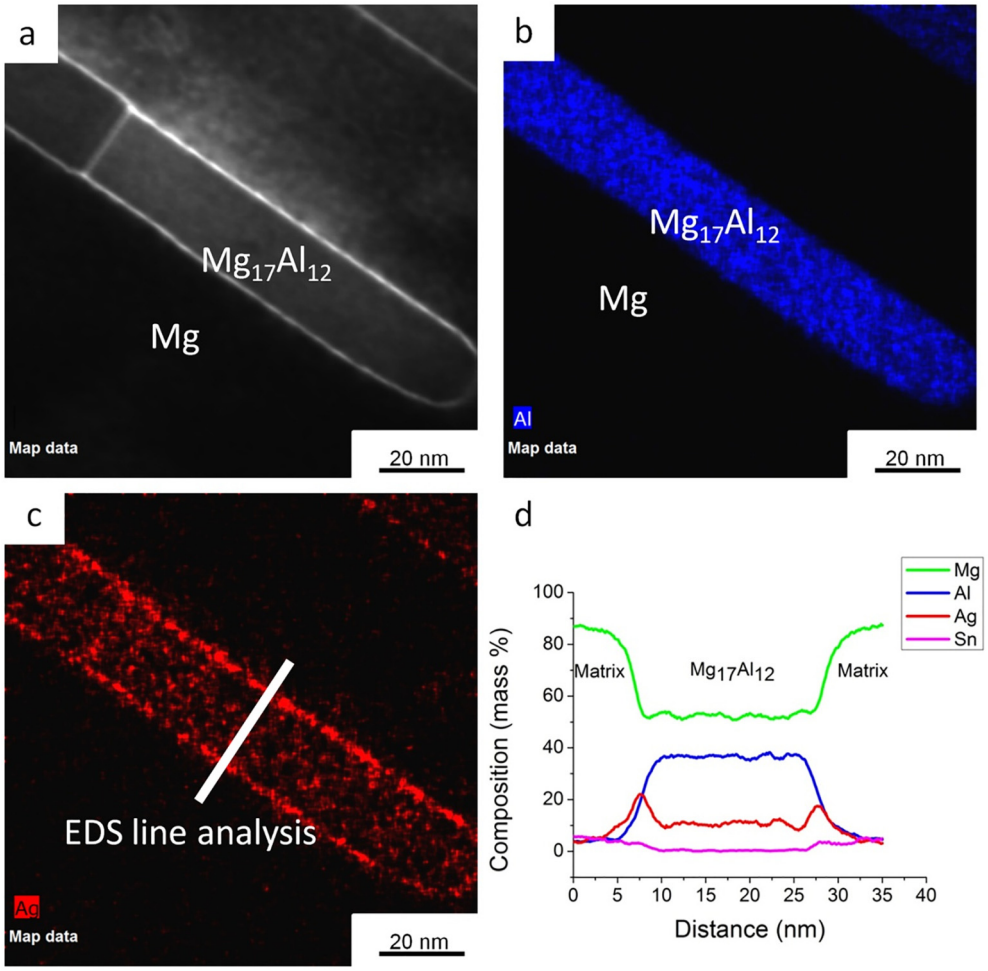

Fig. 4. STEM-EDS characterization of the solute distribution at interface boundary between $Mg_{17}Al_{12}$ precipitates and magnesium matrix in AT72-0.7 wt% Ag alloy after aging at 200 °C for 55 h: a) STEM image of the region for EDS maps; b) Al map; c) Ag map; and d) integrated EDS composition profiles across a $Mg_{17}Al_{12}$ precipitate.

Table 1
Quantitative measurements of three dimensional sizes and number density of continuous $Mg_{17}Al_{12}$ precipitates in AT 72 alloy and AT72-0.7 wt% Ag alloy after isothermal aging at 200 °C for 55 h.

Alloy	Mean thickness (nm)	Mean width (nm)	Mean length (nm)	Number density (/μm^3)
AT72	39 ± 18	204 ± 55	1050 ± 433	5 (ion milling foils), 2.2 (FIB foil)
AT72–0.7.wt% Ag	18 ± 6	63 ± 25	373 ± 178	65 (ion milling foils), 46 (FIB foil)

was observed in Mg-Y-Zn [14], Mg—Zn [15], Mg—Gd [16,17] and Mg—Sn [18] alloys, with small additions of Ag. Such improvement in aging response in these alloys is mainly attributed to precipitate refinement and increased precipitate number density. However, the role of Ag addition in controlling precipitate refinement is still not well understood. Previous study shows that Zn addition can substantially improve the aging hardening response of Mg—Sn alloy through refining precipitates [10,11]. Recently, using advanced scanning transmission electron microscopy combined with STEM-EDS, interphase boundary segregation of Zn is observed at Mg—Sn alloys [12]. The main features of Ag segregation along $Mg_{17}Al_{12}$ precipitates in Mg—Al based alloys observed in this study are similar to those of Zn segregation along Mg_2Sn phase boundaries in Mg—Sn based alloys [12]. Zn segregation at interface boundary between Mg_2Sn may decrease the interfacial energy between precipitate and matrix, thus reducing activation energy barrier to precipitate nucleation and promoting precipitation nucleation rate. On the other hand, reduction in the precipitate-matrix interfacial energy may also help slow down the coarsening process and results in finer precipitates thus improved aging hardening response [12]. Ag segregation at the interface boundary between $Mg_{17}Al_{12}$ and magnesium matrix observed in current study may play a similar role in precipitate refinement.

Mg—Al based alloys represent one group of the most popular magnesium alloys currently available for commercial applications. $Mg_{17}Al_{12}$ precipitation makes a crucial contribution to the strength of this group of alloys. Current study shows that a small amount of Ag addition can remarkably refine $Mg_{17}Al_{12}$ precipitates, thus improving aging hardening response and strength. This finding suggests that microalloying can be an effective way to further improve and optimize the mechanical properties of Mg—Al based alloys.

In summary, with a small addition of Ag, aging hardening response of Mg-7Al-2Sn alloy can be substantially improved. Using advanced STEM coupled with energy-dispersive X-ray mapping, the distribution of solute elements at interphase boundary between $Mg_{17}Al_{12}$ precipitates and magnesium matrix was revealed. For the first time, the segregation of solute element at interphase boundaries of $Mg_{17}Al_{12}$ was identified. As compared with AT72 base alloy, $Mg_{17}Al_{12}$ precipitates in AT72-0.7 wt% Ag are substantially refined and number density of $Mg_{17}Al_{12}$ increases. Such refined and higher density of $Mg_{17}Al_{12}$ precipitates may be responsible for the observed enhanced aging hardening response.

The authors gratefully acknowledge the financial support from the US Department of Energy, under Grant DEEE0006450.

References

[1] T.M. Pollock, Science 328 (2010) 986.
[2] A.A. Luo, Int. Mater. Rev. 49 (2004) 13.
[3] J.F. Nie, Metall. Mater. Trans. A. 43 (2012) 3891.
[4] J.B. Clark, Acta Metall. 16 (1968) 141.
[5] D. Duly, J.P. Simon, Y. Brechet, Acta Metall. Mater. 43 (1995) 101.
[6] S. Celotto, Acta Mater. 48 (2000) 1775.
[7] M.X. Zhang, P.M. Kelly, Scripta Mater. 48 (2003) 647.
[8] A.L. Bowles, C. Blawert, N. Hort, K.U. Kainer, in: A.A. Luo (Ed.), Magnesium Technology, TMS, Warrendale 2004, pp. 307–310.
[9] A.A. Luo, P. Fu, L. Peng, X. Kang, Z. Li, T. Zhu, Metall. Mater. Trans. A. 43 (2011) 360.
[10] C.L. Medis, C.J. Bettles, M.A. Gibson, C.R. Hutchinson, Mater. Sci. Eng. A 435-436 (2006) 163.
[11] T.T. Sasaki, K. Oh-Ishi, T. Ohkubo, K. Hono, Scripta Mater. 55 (2006) 251.
[12] C. Liu, H. Chen, J.F. Nie, Scripta Mater. 123 (2016) 5.
[13] J.F. Nie, Y.M. Zhu, J.Z. Liu, X.Y. Fang, Science 340 (2013) 957.
[14] Y.M. Zhu, A.J. Morton, J.F. Nie, Scripta Mater. 58 (2008) 525.
[15] C.L. Mendis, K. Oh-Ishi, K. Hono, Scripta Mater. 57 (2007) 485.
[16] X. Gao, J.F. Nie, Scripta Mater. 58 (2008) 619.
[17] K. Yamada, H. Hoshikawa, S. Maki, T. Ozaki, Y. Kuroki, S. Kamado, Y. Kojima, Scripta Mater. 61 (2009) 636.
[18] X. Huang, Y. Du, W. Li, Y. Chai, W. Huang, J. Alloys Compd. 696 (2017) 850.
[19] S.J. Pennycook, D.E. Jesson, Ultramicroscopy 37 (1991) 14.
[20] R.J.M. Payne, N. Bailey, J. Inst. Met. 88 (1960) 417.
[21] C.L. Mendis, K. Oh-Ishi, Y. Kawamura, T. Honma, S. Kamado, K. Hono, Acta Mater. 57 (2009) 749.
[22] J.H. Auld, J.T. Vietz, I.J. Polmear, Nature 209 (1966) 703.
[23] S.P. Ringer, K. Hono, I.J. Polmear, T. Sakurai, Acta Mater. 44 (1996) 1883.
[24] C.R. Hutchinson, X. Fan, S.J. Pennycook, G.J. Shiflet, Acta Mater. 49 (2001) 2827.